11 Physics of Biological Systems

C. Andreoli, C. Escher, H.-W. Fink, M. Krüger (until October 06), Tatiana Latychevskaia, H. Okamoto (until October 06), Elvira Steinwand (since December 06), G. Stevens (until October 06)

in collaboration with: Jevgeni Ermantraut, Clondiag Chip Technologies (Germany); Dr. Pierre Sudraud, Orsay Physics (France); Prof. John Miao, University of California at Los Angeles (USA); Prof. Dieter Pohl, University of Basel; Prof. Andreas Plückthun, Dr. Peter Lindner, Biochemistry Institute, University of Zurich; Prof. Joachim M. Buhmann, Institute for Computational Science, ETH Zurich; Prof. Bettina Böttcher, European Institute of Molecular Biology (EMBL), Heidelberg; Prof. Andre Geim, Manchester Centre for Mesoscience & Nanotechnology, University of Manchester.

We intent to develop holography with low energy electrons into a tool for structural biology on the single molecule level. Last year we have been able to achieve some milestones towards this goal. One of the realized steps is finding of a solution to the twin image problem. Since the invention of holography by Denis Gabor more that 50 years ago, it has been the general believe that the twin image problem is an intrinsic limitation of Gabor holography. The apparently unavoidable presence of the conjugated image obscures the information extracted from a holographic record. Despite this general belive we invented a numerical algorithm to remove the effect of this conjugated image and are now able to generate twin-image free hologram reconstructions of both amplitude and phase objects. On the experimental side, an improved detector system for low energy electrons allows to record holograms of DNA molecules with total currents less than 1 nA from the point source and 20 ms acquisition time at the hologram detector. This leads to higher interference resolution in electron holograms. Some of our holography work, that of imaging single proteins, has now been embedded into a European NEST (*New Emerging Science and Technologies*) ADVENTURE European programme with our group being the leading partner within a European consortium. Our studies on the energetics of individual DNA molecules have been extended to the investigation of diffusion of individual molecules in the liquid. Temperature dependent experiments of DNA as well as of latex spheres of comparable mass reveal diffusion coefficients as well as activation barriers for diffusion. It turns out that the DNA diffusion coefficient is much less than that of a comparable stiff object of similar mass, while both objects exhibit similar values for the diffusion barrier.

11.1 Holography of single molecules

11.1.1 Solution to the twin image problem[1]

Holography, since its invention by Dennis Gabor (2), has been troubled by the so-called twin image problem limiting the information that can be obtained from a holographic record. Due to symmetry reasons there are always two images appearing in the reconstruction of a hologram and the unwanted out of focus twin image obscures the object. The problem of the twin images is especially pronounced for emission electron as well as for x- and gamma-ray holography, where the source-object distances are small, and the reconstructed images of atoms are very close to their twin images from which they can hardly be distinguished.

The most widely employed approach to address the twin image problem is to record a set of holograms at different wavelengths

(3; 4). However, this method only suppresses but does not eliminate the twin image and is experimentally difficult to implement in particular when it comes to record fragile biological molecules subject to radiation damage. Most of the known numerical reconstruction routines reconstruct either absorbing or phase shifting properties of the recorded objects (5; 6; 7; 8; 9; 10). We show how the two distributions can be reconstructed simultaneously. This is achieved by the presentation of the transmission function in the object plane as $(1 - a(r_{obj})) \exp(-i\varphi(r_{obj}))$, where $a(r_{obj})$ defines the absorbing properties of the object and $\varphi(r_{obj})$ the phase shift introduced by the object with respect to the incident wave. On the other hand, the transmission function in the object plane can be written as $1 + t(r_{obj})$, where 1 corresponds to the transmittance in the absence of the object, and $t(r_{obj})$ is a complex function describing the presence of the object, so:

$$(1 - a(r_{obj})) \exp(-i\varphi(r_{obj})) = 1 + t(r_{obj}) \ . \quad (11.5)$$

Writing the transmission function as $1 + t(r_{obj})$ helps to identify the part of the incident beam which passes the object un-scattered, thus forming the reference wave on the screen $R(r_s)$. The part of the beam scattered by the object gives rise to the object wave on the screen $O(r_s)$. The recorded hologram is reconstructed numerically by multiplication with the simulated reference wave and further backward propagation of the field to the object plane, where the absorption and phase parts can be separated from the transmission function.

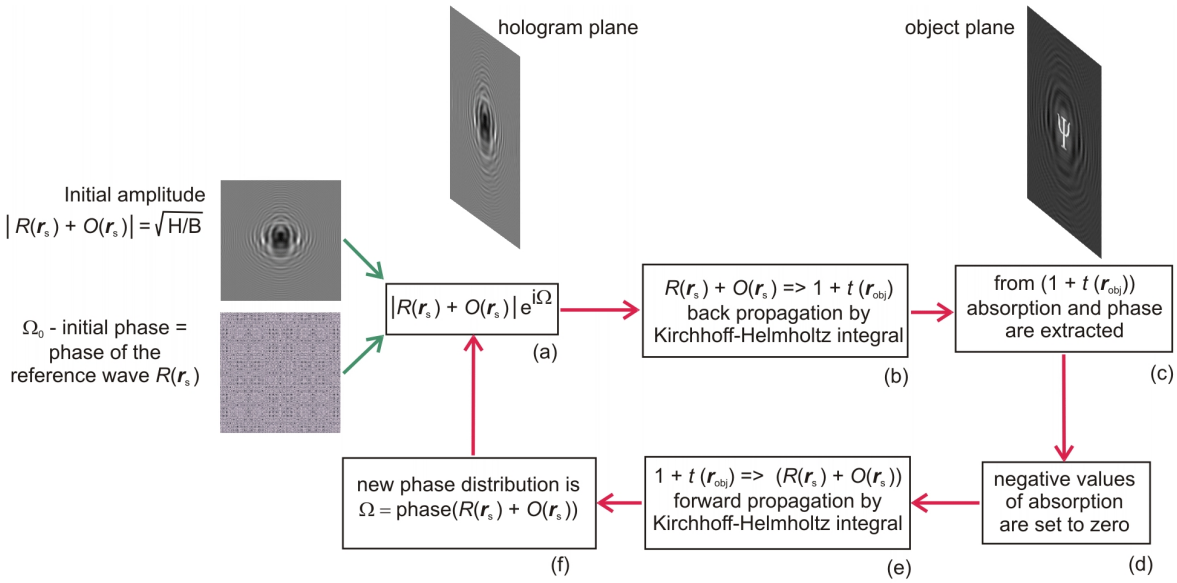

Figure 11.1: Iterative scheme of hologram reconstruction. The amplitude of the complex field in the screen plane is always set as magnitude of the hologram image H divided by the background image B; the initial phase is set to the phase of the reference wave and is iteratively retrieved.
(a) The Complex field in the screen plane is formed.
(b) The field is back propagated to the object plane.
(c) Absorption and phase properties of the object function are extracted.
(d) Negative values of absorption are set to zero.
(e) The field from the updated object function is forward propagated to the hologram plane.
(f) The phase of the propagated field is adopted for step (a) in the next iteration.

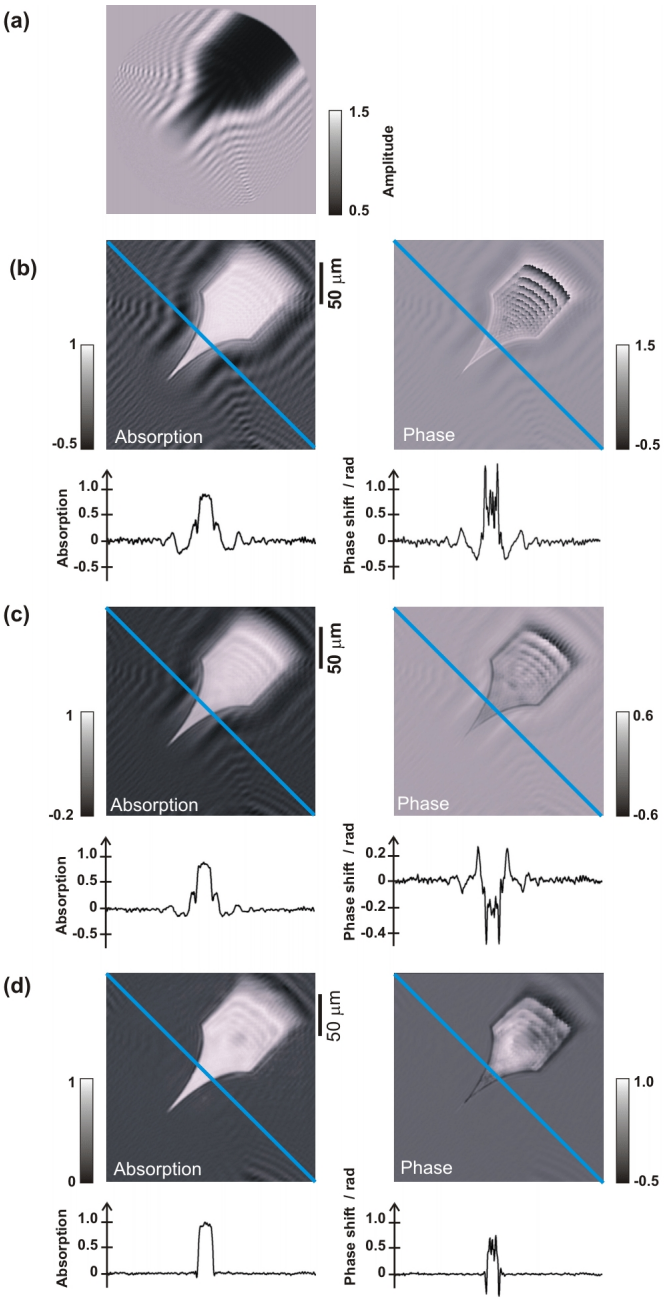

Moreover, we use a filter, which is applied to the reconstructed absorption distribution and sets all negative values to zero. The basic physical notion behind this is the principle of energy conservation. Since negative absorption values would correspond to increased amplitude following a scattering process, we suppress them by replacing them with zeros. Using this filter in an iterative process, shown in Fig. 11.1, the truthful amplitude and phase distributions of the object are retrieved, and the twin image disappears.

Twin-image free reconstructions of simulated and experimental holograms have been obtained for both, strongly absorbing objects, like a metal tip, see Fig. 11.2, as well as for weak scattering, mainly phase shifting objects, like micron sized latex spheres on a glass substrate, see Fig. 11.3.

Our algorithm of reconstructing a hologram completely free of the twin image disturbances is general; no assumptions about the object need to be imposed. Objects can be of arbitrary shape, exhibiting absorbing and/or phase shifting properties. Moreover, the method can be applied to any type of holography independent of the wavelength used and the nature of the wave, be it visible light, x-rays, electrons or any other coherent radiation.

Figure 11.2: Iteratively reconstructed experimental optical hologram of a tungsten tip etched from a 0.1 mm diameter wire.
(a) Normalized hologram.
(b) Reconstructed absorption and phase distributions by conventional reconstruction.
(c) Reconstructed absorption and phase distributions after the first iteration. The oscillations due to the twin image are apparent.
(d) Reconstructed amplitude and phase distributions after 500 iterations.
Below each reconstruction the intensity distributions along the blue lines are displayed. A round cosine window filter was applied to the hologram to avoid artefacts from edges while Fourier-transforming.

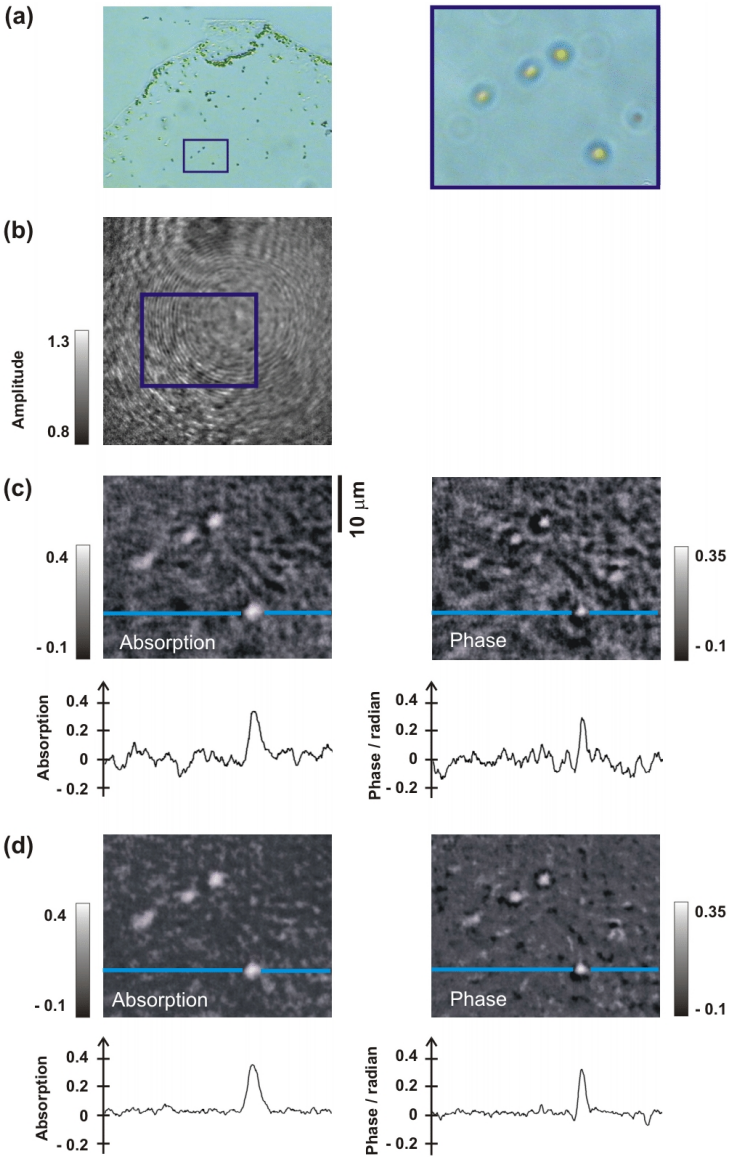

Figure 11.3: Iteratively reconstructed experimental optical hologram of latex spheres of 1 micrometer in diameter.
(a) Conventional optical micrograph of latex spheres deposited onto a glass coverslip. The area marked in blue and magnified at the right was subject to the divergent laser beam to generate the holograms.
(b) Normalized hologram.
(c) Reconstructed absorption and phase distributions by conventional reconstruction.
(d) Reconstructed amplitude and phase distributions after 500 iterations. The phase shifting properties of the spheres are recovered iteratively.
Below each reconstruction the intensity distributions along the blue lines are displayed.

[1] T. Latychevskaia and H.-W. Fink, Solution to the Twin Image Problem in Holography, Phys.Rev.Lett., in press.
[2] D. Gabor Nature, 161 (1948) 777-778.
[3] S. Y. Tong, H. Hua Li, and H. Huang, Phys.Rev.Lett.67, 3102 (1991).
[4] J. J. Barton, Phys.Rev.Lett.67, 3106 (1991).
[5] K. A. Nugent, Opt. Comm. 78, 293 (1990).
[6] G. Liu and P. D. Scott, J. Opt. Soc. Am. 4, 159 (1987).
[7] L. Onural and P. D. Scott, Opt. Eng. 28, 1124 (1987).
[8] X. M. H. Huang, J. M. Zuo, and J. C. H. Spence, Appl. Surf. Sci. 148, 229 (1999).
[9] J. F. Arocena, T. A. Rotwell, and M. R. A. Shegelski, Micron 36, 23 (2005).
[10] A. L. Bleloch, A. Howie, and E. M. James, Appl. Surf. Sci. 111, 180 (1997).

11.1.2 DNA holography, radiation damage

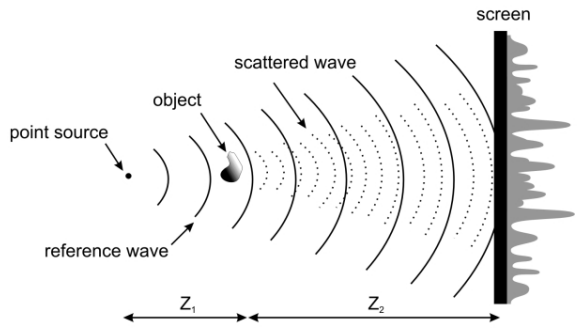

Figure 11.4: Schematic diagram of a LEEPS Microscope: A sharp W-tip acts as a field emitting electron point source of coherent spherical electron waves (20-300 eV). The sample is typically a few microns away from the point source. An electron hologram is formed on a screen located at a macroscopic distance from the specimen by the interference of a scattered electron wave (dotted line) and un-scattered reference electron wave.

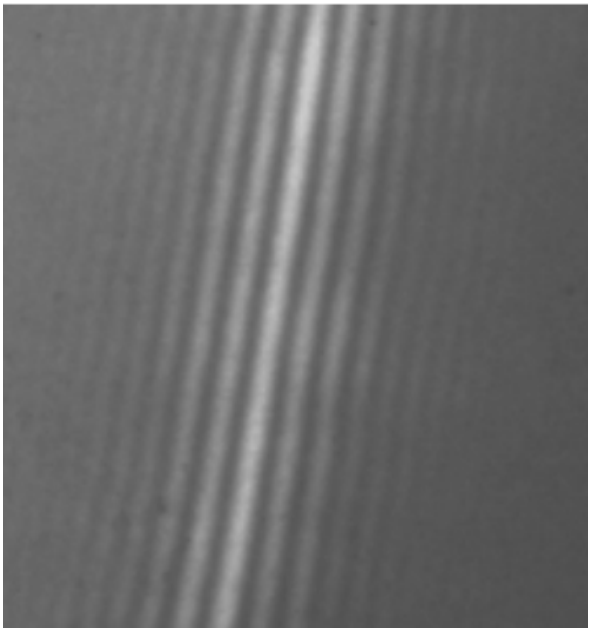

Figure 11.5: A hologram of a multi-walled carbon nanotube (MWNT) is shown at the right part. The MWNT is lying across a micron-sized hole so that the reference wave can pass by the specimen undisturbed.

The basic setup of a (LEEPS) microscope is shown schematically in Fig. 11.4. In this lens-less microscope, images of molecules are obtained by placing them near a point source of coherent electrons in vacuum so that a divergent beam passes by the molecule onto a detector screen located some distance away where a $10^5 - 10^6$ times magnified image is observed. This is precisely the set-up envisioned by Gabor, the inventor of the principle of holography. A hologram as shown in Fig. 11.5 is then created by the interference between object- and reference wave. In contrast to diffraction techniques, like x-ray crystallography in which the phase information is a priori unknown, holograms contain all the phase and amplitude information necessary to reconstruct the original object in three dimensions. Reconstructions are obtained by applying the Kirchhoff-Helmholtz transform to the hologram. Experimental holograms of filamentous macromolecules such as DNA (1) and phthalocyanine polysiloxane (PcPS) (2) have been obtained at electron energies of 50 eV and 70 eV respectively and images of single DNA and PcPS macromolecules were reconstructed from the holograms at a resolution of approximately 2 nm. No observable electron beam damage occurred to the molecules at these energies.

A vital aspect is the need to observe a single molecule for a sufficiently long time to acquire a high resolution hologram but without causing radiation damage. Preliminary experiments with single DNA molecules clearly indicate that there are energy ranges at which neither inelastic scattering nor radiation damage is detectable. Evidence for that is provided in Fig. 11.6 in which a DNA molecule is shown after continuous exposure to low energy electrons for more than 1 hour.

[1] H.-W. Fink, H. Schmid, E. Ermantraut, T. Schulz, J. Opt. Soc. Am. A, 14 (1997) 2168.

[2] A. Gölzhäuser et al., J. Vac. Sci. Technol. A, 16 (1998) 3025.

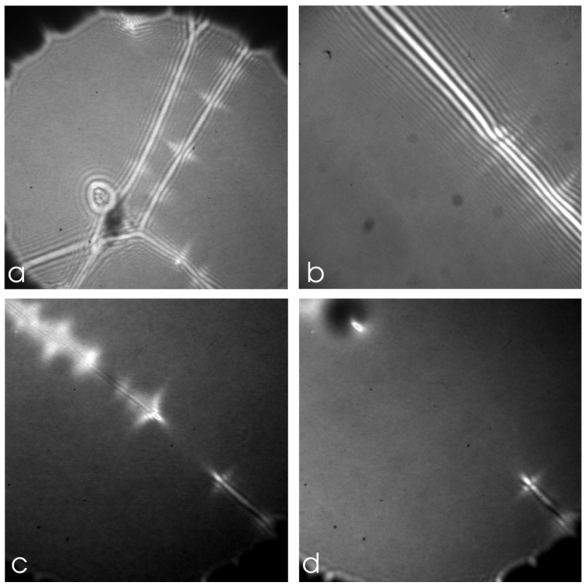

Figure 11.6:
a: Low energy electron hologram of DNA molecules stretched over holes in a thin carbon film.
b: This individual DNA molecule has been imaged and observed for more than one hour being subject to radiation with electrons of energies around 100 eV. No indication for radiation damage occurred.
c: At higher kinetic energies, above 250 eV, radiation damage is apparent.
d: After a few minutes of continuous observation with electrons above 260 eV energy, the DNA strand is found to be decomposed.

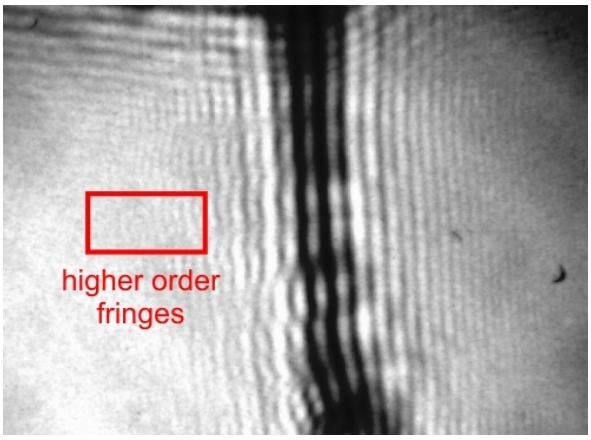

Figure 11.7: A typical noisy experimental electron hologram of a carbon nanotube.

[9]Diploma thesis of Igor Beati

11.1.3 Numerical de-noising of holograms[9]

in collaboration with:
Joachim M. Buhmann, Institute for Computational Science, ETH Zurich.

The holograms recorded with a CCD camera, can be reconstructed numerically by back propagation of the field distribution. The result is a three-dimensional structure monitored on a computer screen. The wavelength of the electron beam (0.1-1 Å) provides sub-nm resolution of the reconstructed objects. One of the problems of numerical reconstruction is associated with the elimination of statistical noise from the holograms. To achieve atomic resolution, higher order interference fringes in holography must be distinguished from noise, see Fig. 11.7. Therefore a numerical pattern recognition routine was developed.

Several de-noising filters were tested:

- Diffusion filter
- Wiener filter
- Median filter
- Wavelets-based filters
- Countourlets based filters
- Coefficients shrinkage-based filters
- Principal components analysis (PCA)-based filter

First, the filters were applied to simulated holograms with superimposed Gaussian noise. The filtered holograms were then compared to simulated noise-free holograms.

As a measure of quality, the peak signal-to-noise ratio (PSNR) has been taken into account. The PSNR is expressed in decibels and it is defined as follows:

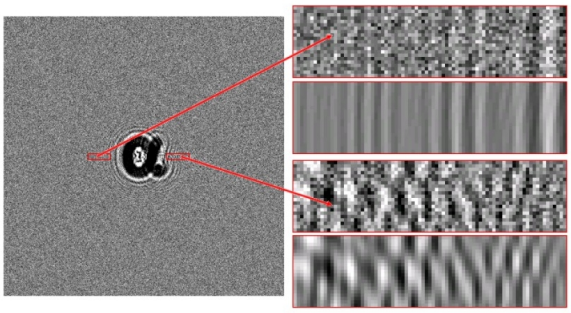

Figure 11.8: Simulated noisy holograms of the letter α (left). On the right side selected areas are shown with (red arrows) and without noise.

$$\mathrm{PSNR} \equiv 10 \times \log \frac{(max(H_0))^2}{MSE} \quad ,$$

where H_0 is the noise-free holographic image, $max(H_0)$ is the maximum pixel value of the image, MSE is the mean squared error of the image defined as

$$MSE \equiv \frac{1}{mn} \sum_{i=0}^{m-1} \sum_{j=0}^{n-1} \|H(i,j) - H_0(i,j)\|^2$$

where H is the noisy holographic image and H_0 is the noise-free holographic image.

Noise-free and noisy holograms of the letter α were simulated and two areas were selected for qualitative analysis, see Fig.11.8.

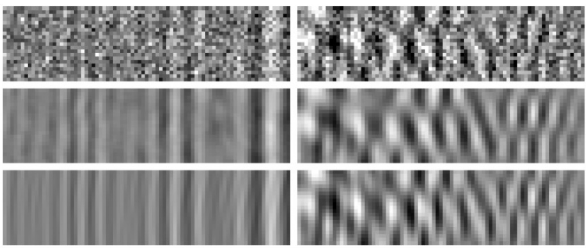

Figure 11.9:
Results of PCA filtering of a noisy hologram. From top to bottom: noisy, de-noised and noise-free.

The best results achieved with the PCA filter are shown in Fig.11.9.

Having defined the most appropriate filter, it was applied to an experimental optical hologram of a phase object, i.e. the letter Ψ engraved in a glass plate. The hologram before and after the de-noising procedure is shown in Fig. 11.10. A significant improvement in terms of identification of individual fringes can be seen on the detail of the hologram.

Fig. 11.11 shows the phase reconstruction. In some regions of the reconstruction of the non-filtered hologram it is impossible to distinguish signal from noise; e.g. regions marked with rectangles A and C. From the reconstruction of the filtered hologram it becomes obvious that the pattern in region A is to be associated with noise, whereas the pattern in region C is to be associated with signal (from the twin image).

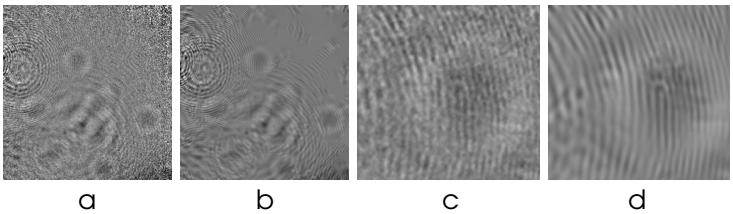

Figure 11.10: Experimental optical hologram of a phase object; a: non-filtered, b: after de-noising with the PCA filter, c and d: details of a and b, respectively.

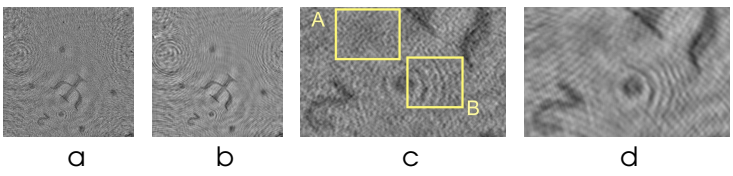

Figure 11.11: Reconstructed phase distributions of the optical hologram shown in Fig. 11.10; Labels defined as in Fig.11.10.

11.1.4 The SIBMAR project

in collaboration with: Gregory Stevens, Peter Lindner and Andreas Plückthun, Biochemistry Institute; Willem Tichelar and Bettina Böttcher, European Molecular Biology Laboratory, Heidelberg; Kostya Novoselov and Andre Geim, University of Manchester.

The main objective of the SIBMAR project is to obtain structural information about individual biological macromolecules at atomic resolution. A consortium with groups headed by Prof. Andre Geim of the University of Manchester and Dr. Bettina Böttcher of the EMBL in Heidelberg has been formed and is funded by the European commission since October 2006. The administrative lead of this project is with the Zurich Euresearch team, Jürg Brunnschweiler and Agate Keller in collaboration with Monika Röllin and Ruth Halter of the Physics Institute. Given the technological and possibly commercial interest, the founder of Clondiag Chip Technologies, Jevgeni Ermantraut, has agreed to assume the role of chairman of the scientific steering committee of SIBMAR. We envision tackling the following sub-objectives:

- An atomically thin carbon support substrate will be developed by the group of Andre Geim.
- The effects of low energy electrons on biological molecules will be studied by Bettina Böttcher's group.
- Andreas Plückthuns group will develop methodologies for preparing individual bio molecules.
- Tatiana Latychevskaia, of our group, will develop numerical reconstruction routines for recovering three-dimensional images from a set of holograms.
- Others in our group will develop a prototype LEEPS microscope for obtaining high resolution holograms.

11.2 Activation barrier for single DNA diffusion from direct measurements of the tracer diffusion coefficient[1]

Molecular transport of bio-molecules in the liquid represents a fundamental issue related to the physics of biological systems. Mobility is a pre-requisite for subsequent interaction such as recognition and binding. The quantity describing such transport in microscopic systems is the diffusion coefficient. Within the last decade, tracking the motion of single DNA molecules in the liquid has become feasible by employing fluorescence video microscopy. Here we present first direct measurements of the energetics involved in self diffusion of a single DNA molecule by observing the random motion of the molecule at different temperatures. Since a DNA molecule is a semi flexible biopolymer, it is not a priori clear how the displacement of the centre of mass actually proceeds. It seems however clear that the Brownian agitation of the solvent frequently leads to rearrangements of the molecules configuration without displacing its centre of mass significantly. For a quantitative evaluation, we have measured both, the diffusion of a stained DNA molecule as well as the diffusion of a rigid fluorescent sphere of 50 nm radius unable to undergo shape changes upon statistical collisions with the solvent. The concentrations are held sufficiently low to allow tracing an individual molecule or sphere reliably. As it turns out the DNA molecule diffuses much slower despite the fact that its mass is an order of magnitude lower than the mass of the rigid sphere; see Fig. 11.12.

According to $< x^2 >= 2Dt$, the mean square displacement reveals the diffusion coefficient. The experimental set up allows observation under thermo dynamical equilibrium conditions at different, well defined temperatures between freezing of the sample and denaturation of the DNA molecule. From the tem-

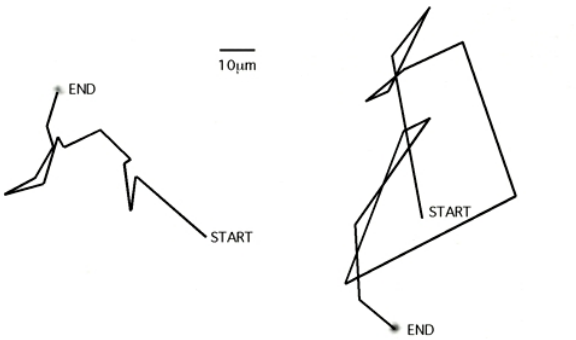

Figure 11.12: Random walk in a thin water film. Left: the displacement of the centre of mass of an individual DNA molecule is traced at time intervals of 30 s. The molecule is stained and embedded in a thin sealed water film. Only a partial sequence (13 out of 50 steps) is depicted here. Right: for comparison the displacement of a styrene sphere with a diameter of 100 nm is monitored under equal conditions.

perature dependence of the diffusion coefficient we compute the activation barrier for self diffusion for both, the DNA molecule and the styrene sphere respectively; see Fig.11.13.

At all measured temperatures we find the diffusion coefficient to be one order of magnitude bigger for the massive (but rigid) sphere than for the light (but filiform) DNA molecule.

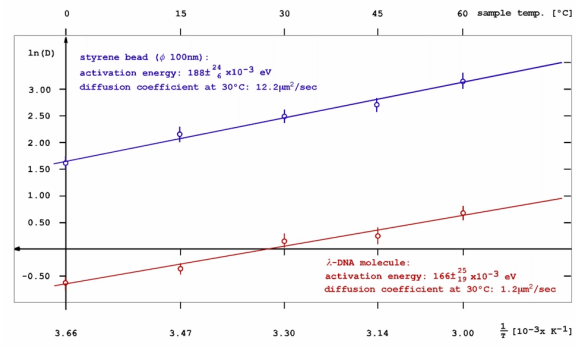

Figure 11.13: Arrhenius plot of the diffusion coefficient. In red: the diffusion coefficient of a single DNA molecule; in blue: the diffusion coefficient of a 50 nm radius styrene sphere at various temperatures. The activation energy for self diffusion is derived from the slope of the linear fit to the data.

However, the activation energy involved in self diffusion is - within the errors - found to be the same for the molecule and the sphere and therefore might have to be assigned solely to the characteristics of the embedding solvent.

[1] Zupfen am Lebensfaden: Experiment mit einzelnen DNS Molekülen, Conrad Escher und Hans-Werner Fink, Physik in unserer Zeit, Heft 4 (2007).

11.3 Coherent low-energy electron diffraction microscopy of single biomolecules

in collaboration with: John Miao, University of California at Los Angeles

This project started in October 2006. The objective is to demonstrate a technique for recording oversampled coherent low-energy electron diffraction patterns of individual biological molecules. From these, the three dimensional structure of the molecule can be recovered at a resolution of 2Å, which is sufficient to show the location of individual atoms in the molecule. The principle of phase retrieval by oversampling, pioneered by J. Miao, D. Sayre, and H.N. Chapman, in which unique phase information about the wave front is recovered from a diffraction pattern, has already been demonstrated experimentally using x-rays and high-energy electrons. However, even with the free electron lasers, currently under construction, averaging over 10^6 molecules is necessary due to the dominating inelastic scattering of x-rays.

The novel aspect of this project is to use low-energy electrons to obtain the diffraction pattern of a single molecule. In contrast to high-energy electrons and x-rays, electrons with energies below 200 eV do not appear to

damage individual biological molecules since elastic scattering dominates.

Experimentally, diffraction patterns will be obtained by using coherent low-energy electrons passing by a single freestanding biological molecule positioned across a hole of a few 10 nm in diameter. Therefore, a parallel coherent electron beam must be formed and directed towards the molecule. The fine structure of the resulting coherent diffraction pattern must be recorded with high detector resolution to fulfil the oversampling criteria. For recovering the 3-dimensional structure of the molecule at atomic resolution, rotation of the molecule needs to be implemented for recording 3-dimensional diffraction patterns.

The main goal of the project will be accomplished following a clearly laid out plan of experimental work. Specific tasks are:

- To develop an electrostatic micro-lens for creating a parallel electron beam and maintaining a high degree of coherence.
- To develop a methodology for preparing single bio molecules so that they extend out into holes exhibiting diameters of a few 10 nm.
- To design and build a diffraction microscope with a dedicated detector system optimised for obtaining oversampled diffraction patterns.

If successful, this technique has the potential to be used for obtaining structural information about all biological molecules, rather than a small subset that is currently accessible by x-ray crystallography or NMR spectroscopy.

11.3.1 The over sampling method

J. Miao, D. Sayre, and H.N. Chapman (1) have shown that, provided a diffraction pattern is sampled on a sufficiently fine grid and the surrounding of the molecule is known, an iterative procedure allows recovering the phase information and with this the structure of the molecule. Miao et al. demonstrated that the phase retrieval algorithm converges after a couple of thousand iterations. Below, some details of the method are given.

An object can be described by a three-dimensional complex electron density function. The amplitude of this function describes the object's absorption properties and the phase of this function expresses the phase shift introduced by the object due to elastic scattering of the incident wave. For a non-crystalline sample the diffraction intensity in the far-field forms a continuous pattern. If the pattern is sampled with the Nyquist frequency (inverse of the size of the specimen) N it can be expressed as the amplitude of the Fourier-transform of the object electron density function (2).

$$
\begin{aligned}
&\mid F(k_x, k_y, k_z) \mid = \\
&= \mid \textstyle\sum_{x=0}^{N-1} \sum_{y=0}^{N-1} \sum_{z=0}^{N-1} \rho(x,y,z) e^{2\pi i (k_x + k_y + k_z)/N} \mid \\
&k_x, k_y, k_z = 0, \ldots, N-1 \; .
\end{aligned}
$$

Each pixel of the diffraction pattern is expressed by a Fourier transform through all the unknown values of the object electron density values, which gives rise to a set of equations. When the object electron density function $\rho(x,y,z)$ is complex, then the number of equations is N^3, while the number of unknowns is $2N^3$, for the real and the imaginary part. When $\rho(x,y,z)$ is real the number of equations is $N^3/2$, due to the symmetry of the diffraction pattern. For a unique solution, the number of equations should be equal to the number of unknowns which can be achieved by chosing the sampling number of pixels in the diffraction pattern M^3 with $M = \sqrt[3]{2}N$.

Sampling the diffraction pattern with a larger number of pixels ($M > \sqrt[3]{2}N$) is equivalent to surrounding the object function with zero values. The following parameter is introduced to characterize the degree of oversampling:

$$\sigma = 2\,\frac{\text{volume of } e^{-}\text{density} + \text{volume with } 0'\text{s}}{\text{volume of } e^{-}\text{density}}$$

The condition is than replaced by $M = \mathcal{O}\mathcal{N}$ where $\mathcal{O} = \sqrt[3]{\sigma}$ (3).

The iterative reconstruction procedure (4) includes the following steps, also illustrated in Fig. 11.14:

- The measured magnitude of the diffraction pattern and an arbitrary guessed phase set (random phase set for initial set $(-\pi;\pi)$) are combined.

- An inverse Fourier transform is applied to the combined set and a complex object electron density function is obtained.

- The value of pixels in the area that is expected to be occupied by the object electron density function (S), defined according to the value of σ, are adjusted so that the negative values of the real or imaginary part are set to zero. The values of pixels located outside this area (regions S_1 and S_2) where there should be no object electron density are gradually set to zero according to:

$$\begin{aligned}\rho_{j+1}(x) &= \rho_j(x) - \beta_1\rho'_j(x)\,, \quad x \in S_1\\ &= \rho_j(x) - \beta_2\rho'_j(x)\,, \quad x \in S_2\end{aligned}$$

  Such asymmetrical constraint speeds up the convergence of the algorithm. A forward Fourier transform is applied, and the phase distribution of the obtained result is set as an actualized phase set for step one of the procedure.

At the end of this procedure, two complex fields are obtained: an object electron density and the field distribution in the far-field, which are mutual Fourier transforms of each other. The higher the value of σ the faster the algorithm converges.

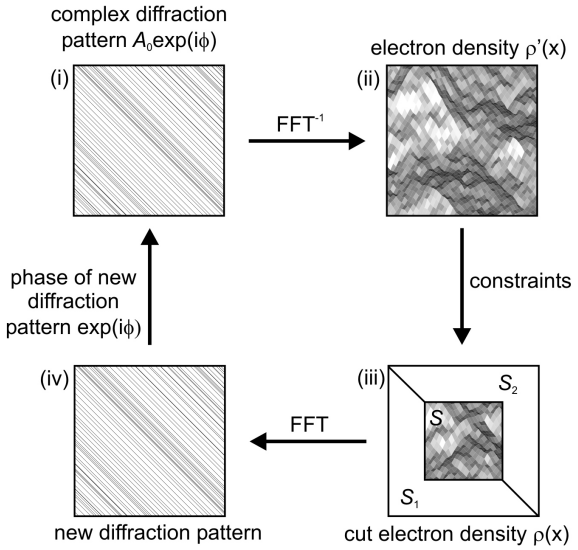

Figure 11.14: An illustration of the iterative reconstruction procedure.
(i) Complex diffraction pattern, where A_0 is the magnitude of the measured diffraction pattern. The phase for the initial phase is randomly distributed.
(ii) By FFT^{-1} the complex electron density is obtained.
(iii) The values surrounding the central part are set to zero.
(iv) FFT gives a new diffraction pattern, whose phase $\exp(i\phi)$ is set as new phase for step (i) [5].

[1] J. Miao, D. Sayre, and H.N. Chapman, J. Opt. Soc. Am. A 16(6) (1998) 1662.
[2] J. Miao, K.O. Hodgson, and D. Sayre, PNAS 98 (2001) 6641.
[3] J. Miao, T. Ishikawa, E.H. Anderson and K.O. Hodgson, Phys. Rev. B 67 (2003) 174104.
[4] J. Miao, D. Sayre, and H.N. Chapman, J. Opt. Soc. Am. A 16(6) (1998) 1662.
[5] J. Miao, D. Sayre, Acta Cryst. A. 56 (2000) 596.

11.3.2 Micro-Lens

An essential experimental aspect is to develop an electrostatic micro lens for generating a parallel electron beam that preserves the spatial coherence of the electron point source beam. A micro lens is required for use with low-energy electrons since the lens aberrations scale with the dimensions of the lens. To maintain coherence, lens aberrations should be several orders of magnitude less than for conventional macroscopic lens. The specifications of the beam are mentioned below. Initial testing of the lens will be done in a LEEPS microscope so that this work can begin while a purpose built low-energy electron microscope is being designed.

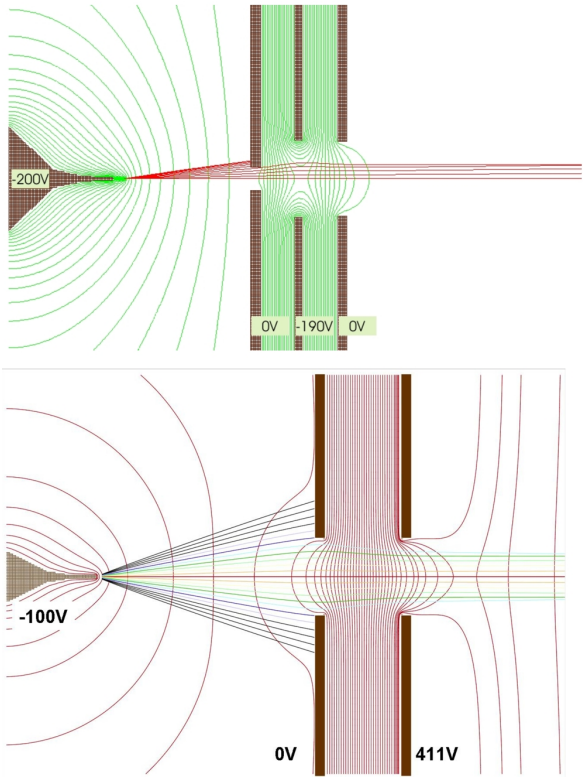

Figure 11.15: SIMION simulation of electron trajectories for an electrostatic lens used to form a parallel beam out of the coherent spherical wave originating from an atomic point source. Top: Einzel lens. Bottom: Two-electrode lens.

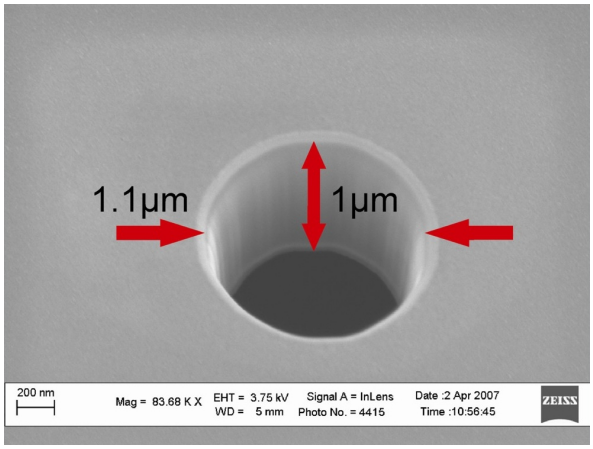

Figure 11.16: SEM image of a micrometer hole in a silicon nitride membrane of 1 μm thickness milled with the FIB. The membrane is covered with Pt layers on both sides.

The lens will be designed with the aid of the ray-tracing software SIMION, which will be used for simulating trajectories of electrons within the microscope. An example of such a simulation for a preliminary lens design is shown in Fig.11.15.

To simplify matters a first lens design is based on a two-electrode architecture as shown in Fig. 11.15 (on the botom). It can be made out of a commercially available silicon-nitride membrane, which constitutes an insulating layer. Two conducting layers evaporated on both sides of the membrane form the electrodes. The aperture in the center of the membrane can be structured using a FIB instrument. Figure 11.16 shows such a micrometer hole in a silicon-nitride membrane covered with a platinum layer of about 30 nm on both sides.

11.3.3 Overall system design

The overall system consist of a fixed mounted micro-lens while the electron point source as well as the sample can be manipulated with nm precision to align the three optical elements. The detector consists of a channel

plate - fibre optic plate assembly to transfers the image directly to a high resolution CCD chip. The system shall also be equipped with a secondary electron detector, both for initial alignment of the source with the micron sized first lens aperture and for testing the optical properties of the lens by scanning the focussed beam over a test structure.

11.3.4 Numerical recovery of the molecular structure from diffraction data

Initially, a 2-dimensional image of a bio molecule will be recovered from a single 2-dimensional diffraction pattern. This will be done in collaboration with Prof. J. Miao at the UCLA who will be in Zurich for regular meetings and updates. Dr. Tatiana Latychevskaia, who is responsible in our group for developing the numerical reconstruction software for LEEPS microscopy will also be involved with this aspect of the work. The quality of the reconstructed images will provide feedback about the experimental conditions used to obtain the diffraction pattern and show how the quality of the patterns might be improved.

Ultimately, a set of 2-dimensional diffraction patterns of a molecule will be obtained from a range of angles. This set will then be assembled into a single 3-dimensional diffraction pattern from which the 3-dimensional electron density map of the molecule will be recovered.

11.4 Bachelor studies

Alice Kohli, under the supervision of Gregory Stevens, Conrad Escher and Hans-Werner Fink, has studied in her Bachelor thesis the influence of various environmental conditions on the light emission of the Green Fluorescent Protein (GFP). It has turned out that GFP emits photons even under vacuum conditions provided the molecules are cooled down to liquid nitrogen temperatures.

In relation to our recent invention of a solid electrolyte ion source (1) Matthias Germann, under the supervision of Conrad Escher, Cornel Andreoli and Hans-Werner Fink, has studied the silver ion transport in thin wires of amorphous (AgI)(AgPO3) which is a solid electrolyte. It has been possible to fabricate and electrically characterize thin electrolyte wires. Observations in the Scanning Electron Microscope have also been carried out and showed the formation of bulk silver at the negative pole at which the wire has been contacted by a carbon electrode.

[1] C. Escher, S. Thomann, C. Andreoli, H.-W. Fink, J. Toquant and D.W. Pohl,
Appl. Phys. Lett. 89, 053513 (2006).

11.5 Education

Two physics laboratory assistant apprentices (from ETHZ) spent part of their practical education course in our lab under the guidance of Cornel Andreoli. Apart from a crucible control for the electron beam evaporator that allows automatic selection of the target material, a valve control for the SEM was built to reduce nitrogen gas wastage.